Terminable Transitions in a Topological Fermionic Ladder

Yuchi He,[1,2] Dante M. Kennes,[1,3] Christoph Karrasch,[4] and Roman Rausch[4]

[1] *Institut für Theorie der Statistischen Physik, RWTH Aachen University and JARA—Fundamentals of Future Information Technology, 52056 Aachen, Germany*
[2] *Rudolf Peierls Centre for Theoretical Physics, Clarendon Laboratory, Parks Road, Oxford OX1 3PU, United Kingdom*
[3] *Max Planck Institute for the Structure and Dynamics of Matter, Center for Free Electron Laser Science, 22761 Hamburg, Germany*
[4] *Technische Universität Braunschweig, Institut für Mathematische Physik, Mendelssohnstraße 3, 38106 Braunschweig, Germany*

(Dated: March 1, 2023)

Interacting fermionic ladders are important platforms to study quantum phases of matter, such as different types of Mott insulators. In particular, the D-Mott and S-Mott states hold pre-formed fermion pairs and become paired-fermion liquids upon doping (d-wave and s-wave, respectively). We show that the D-Mott and S-Mott phases are in fact two facets of the same topological phase and that the transition between them is terminable. These results provide a quantum analog of the well-known terminable liquid-to-gas transition. However, the phenomenology we uncover is even richer, as in contrast to the former, the order of the transition can be tuned by the interactions from continuous to first-order. The findings are based on numerical results using the variational uniform matrix-product state (VUMPS) formalism for infinite systems, and the density-matrix renormalization group (DMRG) algorithm for finite systems. This is complemented by analytical field-theoretical explanations. In particular, we present an effective theory to explain the change of transition order, which is potentially applicable to a broad range of other systems. The role of symmetries and edge states are briefly discussed.

A ladder geometry can be thought of as a narrow strip of a two-dimensional lattice, or as a chain endowed with additional local degrees of freedom (the "rungs" of the ladder). Ladders that host interacting fermions are versatile flagship platforms for studying quantum phases and their transitions in one dimension [1–6], such as repulsion-induced pairing [7–14]; or serve as realizations of symmetry-protected topological phases [15–21]. Ladder models also appear for two-orbital chains [22, 23] and effectively for more general quasi-one-dimensional systems, such as nanoribbons [24] and -tubes [25–28].

A particularly interesting aspect is that fermionic ladders realize Anderson's mechanism for superconductivity from repulsive interactions, which was originally proposed for cuprates [11, 29]: An effective exchange interaction at half filling causes fermions to pair up as spin singlets in an insulating Mott phase; these preformed pairs become mobile upon doping. While the physics of cuprates has turned out to be more complicated, the finite extension of the rungs of a ladder strongly favors such a pairing with a particularly strong binding energy [11]. Two pairing patterns can occur on a rung (see Fig. 1): If local repulsion dominates, it avoids double occupancy and promotes singlets across the rung. If local attraction dominates, it favors double occupancy and promotes on-site singlets. Upon doping, these patterns yield superconducting states that have been dubbed "d-wave" and "s-wave", respectively, in analogy to the 2D case [1, 6]. The half-filled insulating states are correspondingly called "D-Mott" and "S-Mott" [4, 6]. It is known that the rung-singlet wavefunction (D-Mott) is a realization of the topological Haldane phase [15, 18, 19, 22].

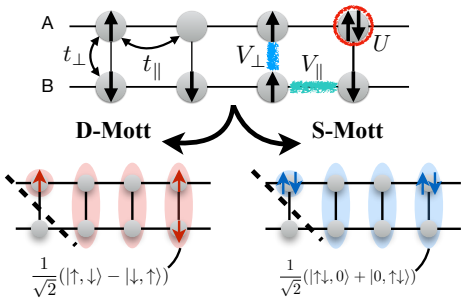

FIG. 1. Top: Illustration of the fermionic ladder, Eq. (1). Bottom: The idealized wavefunctions of the D-Mott (S-Mott) phase are given by product states of rung-singlets (on-site singlets) in the limit of strong local repulsion $U > 0$ (strong local attraction $U < 0$). For open boundary conditions that cut the singlets open (dotted line), edge states are produced that have spin (charge) degrees of freedom. The S-Mott state can be equally achieved by a strong intra-rung repulsion $V_\perp > 0$.

In this work, we study the competition between the two singlet types in more detail and find that a phase transition emerges between the two Mott states, but *the transition line is terminable*. Therefore, D- and S-Mott are adiabatically connected, and one should think of them as *two facets of one and the same topological phase*. This physics also provides a quantum analog of the prototypical, classical liquid-to-gas transition, which is terminable

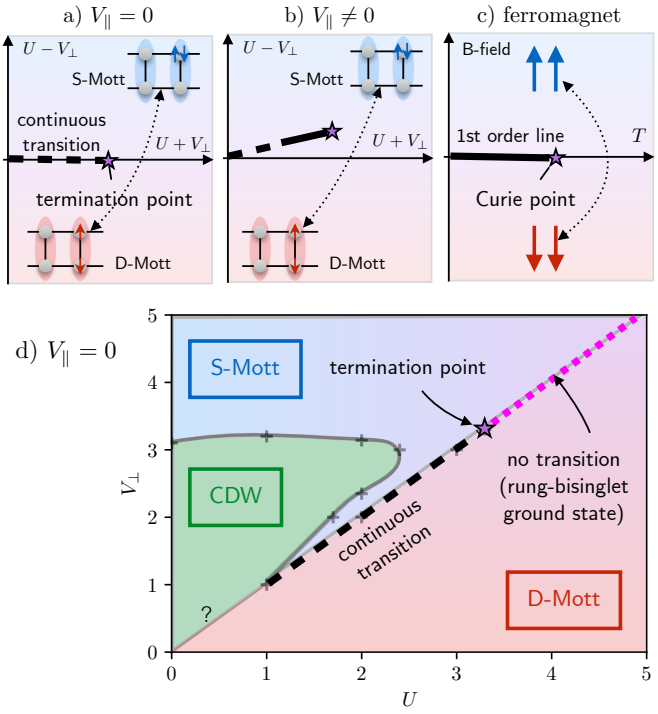

FIG. 2. a), b) Terminable transitions (schematic) of the fermionic ladder. The D-Mott and S-Mott phase (cf. Fig. 1) can be adiabatically connected via a path that avoids the transition line. The transition becomes at least partially first-order for $V_\parallel \neq 0$. c) Paradigm of a terminable transition: a ferromagnet with a B-field at finite temperature T. Below the Curie point, there is a first-order transition when tuning B across zero, but no transition above it. The phases are characterized by: a), b) density difference of D-type and S-type singlets [Eq. (2)]; c) density difference of ↑ and ↓ spins, i.e., magnetic moments. d) Quantitative phase diagram for the model Eq. (1) with $V_\parallel = 0$, computed by VUMPS (CDW: charge density wave). For small interactions, it is unclear if there is a direct transition between D-Mott and CDW marked by "?". The continuous transition terminates at $U = V_\perp \approx 3.4$, after which the gapped exact rung-bisinglet (see text) is the ground state (magenta line). The fate of the transition for $V_\parallel \neq 0$ is shown in Fig. 4.

and of first order (another example is the ferromagnet, cf. Fig. 2). However, we show that the terminable transition in our system is richer in the sense that its order can change from first-order to continuous, depending on the interaction details. This is schematically summarized in Fig. 2. As the effective theory of liquid-to-gas transitions [30] was integral to understand the physics of a wide range of very different systems [31–37], understanding the change of order and robustness of the transition line might take a similarly pronounced role.

Hamiltonian.— We consider the following Hamiltonian of fermions on a ladder (pictorially shown in Fig. 1):

$$\begin{aligned} H = &- \left(\sum_{j,l,\sigma} t_\parallel c^\dagger_{j+1,l,\sigma} c_{j,l,\sigma} + \sum_{j,\sigma} t_\perp c^\dagger_{j,\mathrm{A},\sigma} c_{j,\mathrm{B},\sigma} \right) + h.c. \\ &+ \sum_{j,l} \frac{U}{2} \Delta n_{j,l} \Delta n_{j,l} + \sum_j V_\perp \Delta n_{j,\mathrm{A}} \Delta n_{j,\mathrm{B}} \\ &+ \sum_{j,l} V_\parallel \Delta n_{j,l} \Delta n_{j+1,l}, \end{aligned} \tag{1}$$

where $c_{j,l,\sigma}$ ($c^\dagger_{j,l,\sigma}$) annihilates (creates) a fermion with spin σ at the site j of the leg $l = \mathrm{A}, \mathrm{B}$ of the ladder; $\Delta n_{j,l} = n_{j,l} - 1 = \sum_\sigma c^\dagger_{j,l,\sigma} c_{j,l,\sigma} - 1$ is the density deviation from half filling.

The parameters are as follows: $t_\parallel$ ($t_\perp$) is the hopping amplitude along the legs (rungs) of the ladder; similarly $V_\parallel$ ($V_\perp$) is the nearest-neighbor Coulomb interaction along the legs (rungs); U is the local Coulomb interaction. We restrict ourselves to $t_\perp = t_\parallel = 1$ and $U > 0$. While local pairing in the S-Mott phase is commonly discussed in the attractive case $U < 0$, it can also be achieved by setting $V_\perp > 0$ [6] (see Fig. 1). Doing so allows us to study the competition between the two pairing patterns without switching off the interaction. We focus mainly on the U–$V_\perp$ phase diagram and later consider $V_\parallel \neq 0$ to reveal the change of transition order. Finally, we discuss the presence of edge states and the role of symmetry.

To solve the model, we employ the *variational uniform matrix product state* (VUMPS) formalism [38, 39], which variationally determines the ground state within the class of matrix-product states in the thermodynamic limit. The central control parameter is the "bond dimension" χ, which reflects the number of variational parameters. This method is able to find ground states of gapped 1D systems to very high accuracy. We exploit the spin-SU(2) and the charge-U(1) symmetry of the underlying problem [40], which allows us to reach bond dimensions of up to $\chi \sim 10^4$ in the difficult small-gap regions. To look at edge states, we employ the related density-matrix renormalization group algorithm for finite systems [41].

Various aspects of the model Eq. (1) have been studied in different parameter regimes. For $V_\perp = V_\parallel = 0$, the main focus has been on the d-wave pairing [7–10, 12, 14, 42, 43], but also on the excitations [44, 45] and the topological properties [15–18]. For $V_\perp = V_\parallel \neq 0$, the onset of charge order was studied [46, 47]. With analytical methods, phase diagrams have been proposed for various parameter ranges [3–6, 48, 49]. However, the termination of the D-Mott/S-Mott transition and the physics surrounding it have not been revealed in these works.

Results for $V_\parallel = 0$.— A continuous phase transition resulting from gap closure can be detected via a divergent correlation length ξ, which can be extrapolated for

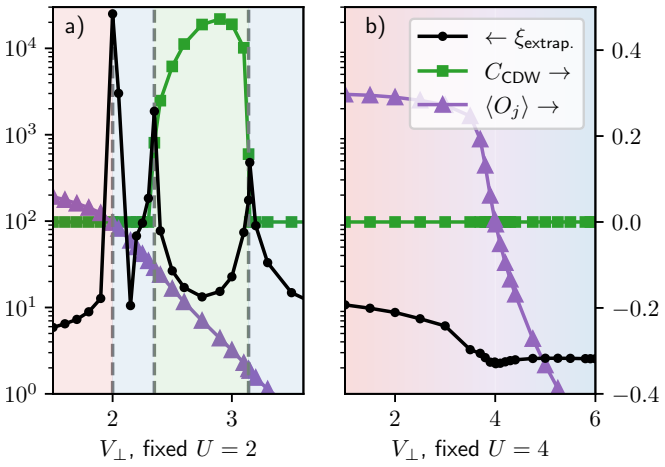

FIG. 3. Extrapolated correlation lengths (left scale) and order parameters (right scale) along a) $U = 2$; b) $U = 4$ for $V_\parallel = 0$. Charge density wave order parameter: $C_{\text{CDW}} = 1/2 \left| \langle n_{j,\text{A}} \rangle - \langle n_{j,\text{B}} \rangle \right|$. For the singlet density difference $\langle O_j \rangle$, see Eq. (2).

the infinite system within the matrix-product state formalism [50, 51]. (A direct computation of the gap for finite systems yields consistent results [51]). Using this method at a fixed $U = 2$ shown in Fig. 3 (a) reveals three transitions as a function of $V_\perp$. We can readily identify a charge density wave (CDW, green area) by its order parameter. It breaks lattice symmetry and is irrelevant for our further discussion. The other phases do not break any symmetries and we argue that they can be identified as S-Mott and D-Mott. To this end, we introduce a microscopic order parameter, namely the "singlet density difference" $\langle O_j \rangle$:

$$\begin{aligned} O_j &= n_{j\text{D}} - n_{j\text{S}} = \Delta^\dagger_{\text{D}j} \Delta_{\text{D}j} - \Delta^\dagger_{\text{S}j} \Delta_{\text{S}j}, \\ \Delta_{\text{D}j} &= (c_{j,\text{A},\uparrow} c_{j,\text{B},\downarrow} + c_{j,\text{B},\uparrow} c_{j,\text{A},\downarrow})/\sqrt{2}, \\ \Delta_{\text{S}j} &= (c_{j,\text{A},\uparrow} c_{j,\text{A},\downarrow} + c_{j,\text{B},\uparrow} c_{j,\text{B},\downarrow})/\sqrt{2}. \end{aligned} \tag{2}$$

This is motivated by the picture that D- and S-Mott phases host immobile preformed d- and s-wave pairs [4], which are characterized by cross-rung pairing ("D") and on-site pairing ("S") [1] (cf. Fig. 1). The corresponding pair annihilation operators are $\Delta_{\text{D}j}$ and $\Delta_{\text{S}j}$. In the strongly-coupled limit of independent rungs, the prototype states can be constructed as $|\text{D}\rangle = \prod_j \Delta^\dagger_{\text{D}j} |\Omega\rangle$ and $|\text{S}\rangle = \prod_j \Delta^\dagger_{\text{S}j} |\Omega\rangle$ [6], where $|\Omega\rangle$ is the vacuum state (see Fig. 1). Therefore, $\langle O_j \rangle > 0$ (< 0) measures that there are more rung (local) singlets in the admixture of the wavefunction and we expect a sign change across the phase transition. In Fig. 3 (a), we see that $\langle O_j \rangle$ indeed switches sign at the gap closure for $U = V_\perp = 2$.

The full phase diagram is shown in Fig. 2. We find a phase transition line between D-Mott and S-Mott along $U = V_\perp$, and a central result is that it terminates at $U = V_\perp \approx 3.4$. Our data show no gap closing and no obvious discontinuity for large U (cf. $U = 4$ in Fig. 3 b), implying that there is an adiabatic path connecting the two Mott phases.

Next, we provide semi-analytical arguments for why the critical line exists exactly along the $U = V_\perp$ and terminates above some value. The two degrees of freedom (A, B) for each rung give rise to two transverse subbands, and it turns out that the particle numbers in each of these subbands are conserved for $U = V_\perp$. To see it, we introduce the transverse subband basis $c_{j,k_y,\sigma}$ defined as $c_{j,0,\sigma} = (c_{j,\text{A},\sigma} + c_{j,\text{B},\sigma})/\sqrt{2}$ and $c_{j,\pi,\sigma} = (c_{j,\text{A},\sigma} - c_{k,\text{B},\sigma})/\sqrt{2}$, where $k_y = 0, \pi$ is the transverse momentum. Rewriting the Hamiltonian Eq. (1) for $V_\parallel = 0$ in this basis, we obtain

$$\begin{aligned} H = &- t_\parallel \sum_{j,k_y,\sigma} (c^\dagger_{j,k_y,\sigma} c_{j+1,k_y,\sigma} + h.c.) - t_\perp \sum_j (n_{j,\pi} - n_{j,0}) \\ &+ U/2 \sum_j (\Delta n_{j,\pi} + \Delta n_{j,0})^2 - (U - V_\perp) H_{\text{res}}, \end{aligned} \tag{3}$$

where $n_{j,k_y} = \sum_\sigma c^\dagger_{j,k_y,\sigma} c_{j,k_y,\sigma}$. The residual term $\propto H_{\text{res}}$ vanishes for $U = V_\perp$, so that $N_\pi = \sum_j n_{j,\pi}$ and $N_0 = \sum_j n_{j,0}$ become conserved.

The Lieb-Schultz-Mattis Theorem [52, 53] states that for a fractional filling factor, the system must be gapless as long as there is no spontaneous breaking of translational symmetry. Our numerics show that the filling ratio $\langle n_{j,\pi} \rangle$ and $\langle n_{j,0} \rangle$ are fractional along $U = V_\perp$ below the termination point. Above the termination point, the fillings are integer with $\langle n_{j,\pi} \rangle = 0$ and $\langle n_{j,0} \rangle = 1$, supporting the termination of the phase transition line. The data are given in the supplemental material [51].

Another perspective for the termination comes from introducing a product state of equal-weight superpositions of the two singlet types: $\prod_j 1/\sqrt{2}(\Delta^\dagger_{\text{S}j} + \Delta^\dagger_{\text{D}j})|\Omega\rangle$, which we dub "rung bisinglet". It is straightforward to prove analytically that the rung bisinglet is always an eigenstate of the model for $U = V_\perp$, though not necessarily the ground state. Our numerics indicate that it becomes the gapped unique ground state above the termination point (Fig. 2).

Results for $V_\parallel \neq 0$.— Next, we show that for $V_\parallel \neq 0$, the above accidental symmetry is lifted and the terminable continuous transition can be replaced by a first-order transition. To suppress the intervening CDW phase, we consider a negative $V_\parallel = -0.1$. Our numerical data (Fig. 4) show that at intermediate U, there is a first-order transition, exhibiting a jump in $\langle O_j \rangle$. For larger U, the transition is absent. For smaller U, the zero crossing is extremely shallow and our numerics cannot distinguish between a very small jump or no jump, so a continuous transition is still possible.

Explaining the change of transition order.— The change of transition order for $V_\parallel \neq 0$ is a feature of our

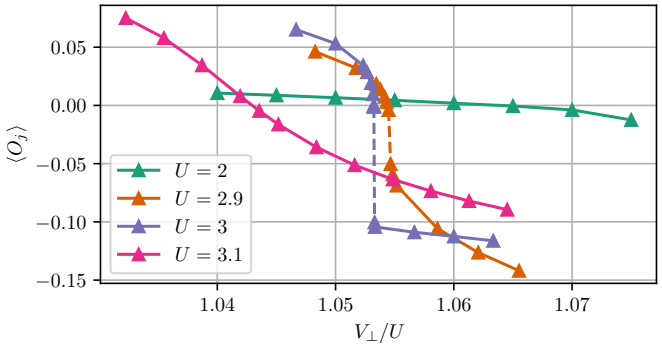

FIG. 4. Ground-state expectation $\langle O_j \rangle$ for $V_\parallel = -0.1$. Inferred from the data points, solid and dashed lines denote smooth curves and discontinuity, respectively. The discontinuity for $U = 3$ indicates a first-order phase transition.

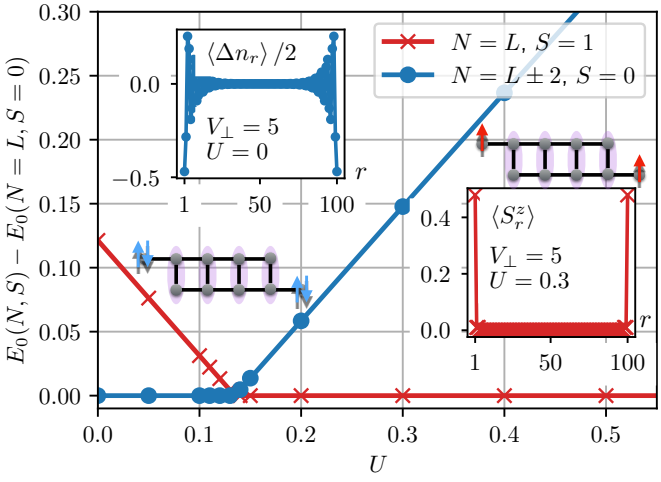

FIG. 5. Ground-state degeneracy and edge modes of open ladders under diagonal cuts. Parameters: number of sites $L = 100$ (i.e. 50 rungs), $V_\perp = 5$, $V_\parallel = 0$. The index $r = 2j + l$ ($l = 0, 1$) consecutively labels the L sites. $E_0(N, S)$ is the lowest energy with N particles and total spin S. The insets show that the edge modes carry spin and charge quantum numbers, respectively. Upper left inset: Particle density $1/2 \langle \Delta n_r \rangle = 1/2 \left(\sum_\sigma \langle c^\dagger_{r\sigma} c_{r\sigma} \rangle - 1 \right)$ in the $N = L - 2, S = 0$ sector. Lower right inset: spin density $\langle S^z_r \rangle = 1/2 \left(\langle n_{r\uparrow} \rangle - \langle n_{r\downarrow} \rangle \right)$ in the $N = L, S = 1$ sector.

system that sets it apart from the conventional liquid-to-gas transition. Moreover, the subband particle number is not conserved anymore for $V_\parallel \neq 0$, raising the question of why a robust transition line still exists in the first place. To investigate this feature more closely, we formulate an effective theory (for details, see [51]), including an analysis of symmetries and scaling dimensions.

The bosonization of continuum operators corresponding to those of Eq. (3) are given by $c_{k_y,\sigma}(x_j) = \frac{\kappa_{k_y,\sigma}}{\sqrt{2\pi}} \sum_{\eta=-1,1} e^{i[\theta_{k_y,\sigma} + \eta(\phi_{k_y,\sigma} + k_{\mathrm{F},k_y\sigma} x_j)]}$, where $\theta_{k_y,\sigma}(x_j)$ and $\phi_{k_y,\sigma}(x_j)$ are dual to each other satisfying $[\theta_{k_y,\sigma}(x,t), \phi_{k'_y,\sigma'}(x',t)] = i\pi\delta_{k_y,k'_y}\delta_{\sigma,\sigma'}\Theta(x - x')$; $\{\kappa_{k_y,\sigma}, \kappa_{k'_y,\sigma'}\} = 2\delta_{k_y,k'_y}\delta_{\sigma,\sigma'}$. The $k_{\mathrm{F},k_y,\sigma}$ is the base wavevector of the low-energy excitation of $c_{j,k_y,\sigma}$. The half-filling condition fixes $k_{\mathrm{F},0,\sigma} + k_{\mathrm{F},\pi,\sigma} = \pi$, where $k_{\mathrm{F},k_y,\sigma}$ is influenced by interaction besides $t_\parallel$ and $t_\perp$. Two-band bosonization requires partially-filled subbands ($k_{\mathrm{F},k_y,\sigma} \neq 0, \pm\pi$). Introducing a transformed basis for the effective fields: $\tilde{\phi}_{c,\pm} = \frac{1}{2}[(\phi_{0,\uparrow} + \phi_{0,\downarrow}) \pm (\phi_{\pi,\uparrow} + \phi_{\pi,\downarrow})]$ and $\tilde{\phi}_{s,\pm} = \frac{1}{2}[(\phi_{0,\uparrow} - \phi_{0,\downarrow}) \pm (\phi_{\pi,\uparrow} - \phi_{\pi,\downarrow})]$, S-Mott and D-Mott has been defined [4, 6] as $\tilde{\phi}_{c,+}$, $\tilde{\phi}_{s,+}$, $\tilde{\phi}_{s,-}$ all locked at 0, and $\tilde{\theta}_{c,-}$ locked at 0 and $\pi/2$ mod π respectively.

We now show the transition line is Gaussian critical where O_j has quasi-long-range order and its scaling dimension indicates the instability of Gaussian criticality to first-order transition when removing the accidental symmetry. When the sectors other than $c, -$ are kept locked, we can approximate the locked fields as constant and obtain

$$O_j \propto -\cos(2\tilde{\theta}_{c,-}(x_j)), \tag{4}$$

whose expectation values flip sign when the locking value $\tilde{\theta}_{c,-} = 0$ changes to $\pi/2$. The discreteness of locking values is related to time-reversal symmetry, as terms like $\cos(2\tilde{\theta}_{c,-}(x_j) + \alpha)$ with continuous varying α is forbidden by it [51]. Near the Gaussian criticality, the effective Hamiltonian density is

$$\mathcal{H}_{c,-} = \frac{v_{c,-}}{2\pi}\left[K(\partial_x\tilde{\theta}_{c,-})^2 + \frac{1}{K}(\partial_x\tilde{\phi}_{c,-})^2\right] + g\cos(2\tilde{\theta}_{c,-}), \tag{5}$$

where K is the Luttinger parameter and $g \propto (V_\perp - U)$ for $V_\parallel = 0$. Equations (4) and (5) can be used to predict the correlator $\langle O_j O_{j+d} \rangle \propto 1/|d|^{2/K}$ at the criticality ($g = 0$). The scaling dimension of O_j is thus $1/K$. Observing non-universal exponents numerically confirms Gaussian criticality; our data [51] suggest $1/K$ goes down from ~ 0.96 to ~ 0.46 when increasing $U = V_\perp$ from 2 to 3.2. As the 0-loop renormalization group relevance criterion is scaling dimension < 2, the measured $1/K$ is consistent with that as long as $g \neq 0$, $\tilde{\theta}_{c,-}$ gets locked.

Now consider $V_\parallel \neq 0$. The term $\cos(2\tilde{\theta}_{c,-})$ could still be absent at a fixed point by accident. However, higher-order terms like $\cos(4\tilde{\theta}_{c,-})$ ($\sim O^2$) generically cannot vanish simultaneously without an exact subband U(1) symmetry. The possible Gaussian criticality requires those terms are irrelevant with the criterion $1/K > 1/2$. Considering the finite U(1) violating term $V_\parallel = -0.1$ as a perturbation, small $1/K$ at the unperturbed criticality indicates that the continuous transition gives way to first-order transition described by a Landau-Ginzburg theory with powers of O.

Edge modes.— With a diagonally cut edge (cf. Fig. 1), the repulsive Hubbard ladder ($U > 0, V_\perp = V_\parallel =$

0) is known to host spin-1/2 edge modes protected by particle-hole symmetry [15, 18, 19]. We find that for our extended model, edge modes can carry either spin or charge quantum numbers, transforming differently under time-reversal symmetry. Intuitively, if on-site singlets (S-Mott) are cut, empty or doubly occupied sites with particle number $N = \pm 2$ remain (see Fig. 5). A change between edge quantum numbers is induced when varying the interaction parameters U and $V_\perp$. From the model wavefunction, one might naively assume that the edge quantum number is directly related to the bulk being D- or S- Mott (i.e. to the sign of $\langle O_j \rangle$), but this is not the case: We find that spinful edge states are strongly preferred, except for very small U. For example, for $V_\perp = 5$, $V_\parallel = 0$, a change in quantum numbers already happens at $U \approx 0.14$ (see Fig. 5), far away from the bulk crossover $U = V_\perp$. Thus, our system provides an example where an edge transition has no bulk indication [54]; though further details are beyond the scope of this study.

Discussion.- We have shown that D- and S- Mott are two facets of the same topological phase. An intuitive explanation is that true d-wave symmetry can only be found on the full 2D square lattice [55]. A terminable transition nevertheless exists without fine-tuning and can be understood with the help of the singlet-density difference. The nature of the transition can change from first order to continuous. We have presented a general effective theory that can capture this feature. The existence of a robust transition itself is assisted by time-reversal symmetry, which sheds light upon the study of robust terminable transitions [54]. We propose that our effective theory may be useful in discovering very different systems with similar transition behavior.

Acknowledgments.— We thank Fabian Essler, Sid Parameswaran, Prakash Abhishodh for discussion. YH and DMK are supported by the Deutsche Forschungsgemeinschaft (DFG, German Research Foundation) under RTG 1995, within the Priority Program SPP 2244 "2DMP" and under Germany's Excellence Strategy - Cluster of Excellence Matter and Light for Quantum Computing (ML4Q) EXC 2004/1 - 390534769. We acknowledge support by the Max Planck-New York City Center for Nonequilibrium Quantum Phenomena. The numerical calculations have been partially performed with computing resources granted by RWTH Aachen University under project rwth0726.

[1] T. Giamarchi, *Quantum physics in one dimension*, International series of monographs on physics (Clarendon Press, Oxford, 2004).
[2] E. Dagotto and T. M. Rice, Surprises on the way from one- to two-dimensional quantum magnets: The ladder materials, Science **271**, 618 (1996).
[3] L. Balents and M. P. A. Fisher, Weak-coupling phase diagram of the two-chain hubbard model, Phys. Rev. B **53**, 12133 (1996).
[4] H.-H. Lin, L. Balents, and M. P. A. Fisher, Exact SO(8) symmetry in the weakly-interacting two-leg ladder, Phys. Rev. B **58**, 1794 (1998).
[5] C. Wu, W. Vincent Liu, and E. Fradkin, Competing orders in coupled luttinger liquids, Phys. Rev. B **68**, 115104 (2003).
[6] M. Tsuchiizu and A. Furusaki, Generalized two-leg Hubbard ladder at half filling: Phase diagram and quantum criticalities, Phys. Rev. B **66**, 245106 (2002).
[7] E. Dagotto, J. Riera, and D. Scalapino, Superconductivity in ladders and coupled planes, Phys. Rev. B **45**, 5744 (1992).
[8] R. M. Noack, S. R. White, and D. J. Scalapino, Correlations in a Two-Chain Hubbard Model, Phys. Rev. Lett. **73**, 882 (1994).
[9] R. M. Noack, S. R. White, and D. J. Scalapino, The doped two-chain hubbard model, Europhysics Letters **30**, 163 (1995).
[10] R. M. Noack, N. Bulut, D. J. Scalapino, and M. G. Zacher, Enhanced $d_{x^2-y^2}$ pairing correlations in the two-leg Hubbard ladder, Phys. Rev. B **56**, 7162 (1997).
[11] S. Chakravarty and S. A. Kivelson, Electronic mechanism of superconductivity in the cuprates, C_{60}, and polyacenes, Phys. Rev. B **64**, 064511 (2001).
[12] Y. Gannot, Y.-F. Jiang, and S. A. Kivelson, Hubbard ladders at small u revisited, Phys. Rev. B **102**, 115136 (2020).
[13] Y.-H. Zhang and A. Vishwanath, Pair-density-wave superconductor from doping haldane chain and rung-singlet ladder, Phys. Rev. B **106**, 045103 (2022).
[14] S. Hirthe, T. Chalopin, D. Bourgund, P. Bojović, A. Bohrdt, E. Demler, F. Grusdt, I. Bloch, and T. A. Hilker, Magnetically mediated hole pairing in fermionic ladders of ultracold atoms, Nature **613**, 463 (2023).
[15] P. Sompet, S. Hirthe, D. Bourgund, T. Chalopin, J. Bibo, J. Koepsell, P. Bojović, R. Verresen, F. Pollmann, G. Salomon, C. Gross, T. A. Hilker, and I. Bloch, Realizing the symmetry-protected haldane phase in fermi–hubbard ladders, Nature **606**, 484 (2022).
[16] F. Anfuso and A. Rosch, String order and adiabatic continuity of Haldane chains and band insulators, Phys. Rev. B **75**, 144420 (2007).
[17] S. Moudgalya and F. Pollmann, Fragility of symmetry-protected topological order on a hubbard ladder, Phys. Rev. B **91**, 155128 (2015).
[18] S. R. White, Equivalence of the antiferromagnetic heisenberg ladder to a single s=1 chain, Phys. Rev. B **53**, 52 (1996).
[19] R. Verresen, R. Moessner, and F. Pollmann, One-dimensional symmetry protected topological phases and their transitions, Phys. Rev. B **96**, 165124 (2017).
[20] W. P. Su, J. R. Schrieffer, and A. J. Heeger, Solitons in Polyacetylene, Phys. Rev. Lett. **42**, 1698 (1979).
[21] F. D. M. Haldane, Nonlinear Field Theory of Large-Spin Heisenberg Antiferromagnets: Semiclassically Quantized Solitons of the One-Dimensional Easy-Axis Néel State, Phys. Rev. Lett. **50**, 1153 (1983).
[22] H. Nonne, E. Boulat, S. Capponi, and P. Lecheminant, Competing orders in the generalized Hund chain model at half filling, Phys. Rev. B **82**, 155134 (2010).

[23] V. Bois, S. Capponi, P. Lecheminant, M. Moliner, and K. Totsuka, Phase diagrams of one-dimensional half-filled two-orbital SU(N) cold fermion systems, Phys. Rev. B **91**, 075121 (2015).

[24] S. Mishra, G. Catarina, F. Wu, R. Ortiz, D. Jacob, K. Eimre, J. Ma, C. A. Pignedoli, X. Feng, P. Ruffieux, J. Fernández-Rossier, and R. Fasel, Observation of fractional edge excitations in nanographene spin chains, Nature **598**, 287 (2021).

[25] L. Balents and M. P. A. Fisher, Correlation effects in carbon nanotubes, Phys. Rev. B **55**, R11973 (1997).

[26] J. E. Bunder and H.-H. Lin, Phase diagrams of the metallic zigzag carbon nanotube, Phys. Rev. B **78**, 035401 (2008).

[27] D. Varsano, S. Sorella, D. Sangalli, M. Barborini, S. Corni, E. Molinari, and M. Rontani, Carbon nanotubes as excitonic insulators, Nature Communications **8**, 1461 (2017).

[28] Moca, Cătălin Paşcu and Izumida, Wataru and Dóra, Balázs and Legeza, Örs and Asbóth, János K. and Zaránd, Gergely, Topologically Protected Correlated End Spin Formation in Carbon Nanotubes, Phys. Rev. Lett. **125**, 056401 (2020).

[29] P. W. Anderson, The resonating valence bond state in La_2CuO_4 and superconductivity, Science **235**, 1196 (1987).

[30] P. M. Chaikin and T. C. Lubensky, *Principles of Condensed Matter Physics* (Cambridge University Press, Cambridge, 1995).

[31] A. Masayuki and Y. Koichi, Chiral restoration at finite density and temperature, Nuclear Physics A **504**, 668 (1989).

[32] L. Xu, P. Kumar, S. V. Buldyrev, S.-H. Chen, P. H. Poole, F. Sciortino, and H. E. Stanley, Relation between the widom line and the dynamic crossover in systems with a liquid–liquid phase transition, Proc. Natl. Acad. Sci. U.S.A. **102**, 16558 (2005).

[33] P. Limelette, A. Georges, D. Jérome, P. Wzietek, P. Metcalf, and J. M. Honig, Universality and critical behavior at the mott transition, Science **302**, 89 (2003).

[34] M. Schüler, E. van Loon, M. Katsnelson, and T. Wehling, Thermodynamics of the metal-insulator transition in the extended hubbard model, SciPost Physics **6**, 067 (2019).

[35] J. L. Jiménez, S. P. G. Crone, E. Fogh, M. E. Zayed, R. Lortz, E. Pomjakushina, K. Conder, A. M. Läuchli, L. Weber, S. Wessel, A. Honecker, B. Normand, C. Rüegg, P. Corboz, H. M. Rønnow, and F. Mila, A quantum magnetic analogue to the critical point of water, Nature **592**, 370 (2021).

[36] A. Sushchyev and S. Wessel, Thermodynamics of the metal-insulator transition in the extended hubbard model from determinantal quantum monte carlo, arXiv preprint arXiv:2205.09512 (2022).

[37] Y. He, K. Yang, M. O. Goerbig, and R. S. K. Mong, Charge density waves and their transitions in anisotropic quantum Hall systems, Communications Physics **4**, 116 (2021).

[38] S. R. White, Density matrix formulation for quantum renormalization groups, Phys. Rev. Lett. **69**, 2863 (1992).

[39] V. Zauner-Stauber, L. Vanderstraeten, M. T. Fishman, F. Verstraete, and J. Haegeman, Variational optimization algorithms for uniform matrix product states, Phys. Rev. B **97**, 045145 (2018).

[40] I. P. McCulloch, From density-matrix renormalization group to matrix product states, Journal of Statistical Mechanics: Theory and Experiment **2007**, P10014 (2007).

[41] U. Schollwöck, The density-matrix renormalization group in the age of matrix product states, Annals of Physics **326**, 96 (2011), january 2011 Special Issue.

[42] G. Karakonstantakis, E. Berg, S. R. White, and S. A. Kivelson, Enhanced pairing in the checkerboard hubbard ladder, Phys. Rev. B **83**, 054508 (2011).

[43] M. Dolfi, B. Bauer, S. Keller, and M. Troyer, Pair correlations in doped hubbard ladders, Phys. Rev. B **92**, 195139 (2015).

[44] Z. Weihong, J. Oitmaa, C. J. Hamer, and R. J. Bursill, Numerical studies of the two-leg hubbard ladder, Journal of Physics: Condensed Matter **13**, 433 (2001).

[45] C. Yang and A. E. Feiguin, Spectral function of mott-insulating hubbard ladders: From fractionalized excitations to coherent quasiparticles, Phys. Rev. B **99**, 235117 (2019).

[46] M. Vojta, R. E. Hetzel, and R. M. Noack, Charge-order transition in the extended Hubbard model on a two-leg ladder, Phys. Rev. B **60**, R8417 (1999).

[47] N. J. Robinson, F. H. L. Essler, E. Jeckelmann, and A. M. Tsvelik, Finite wave vector pairing in doped two-leg ladders, Phys. Rev. B **85**, 195103 (2012).

[48] E. Orignac and R. Citro, Charge density waves and bond orderwaves in a quarter filled extended hubbard ladder, Eur. Phys. J. B **33**, 419 (2003).

[49] M. Tsuchiizu and Y. Suzumura, Charge-density-wave formation in the doped two-leg extended hubbard ladder, J. Phys. Soc. Jpn. **73**, 804 (2004).

[50] M. M. Rams, P. Czarnik, and L. Cincio, Precise extrapolation of the correlation function asymptotics in uniform tensor network states with application to the Bose-Hubbard and XXZ models, Phys. Rev. X **8**, 041033 (2018).

[51] See Supplemental Material.

[52] E. Lieb, T. Schultz, and D. Mattis, Two soluble models of an antiferromagnetic chain, Annals of Physics **16**, 407 (1961).

[53] H. Tasaki, Lieb–schultz–mattis theorem with a local twist for general one-dimensional quantum systems, Journal of Statistical Physics **170**, 653 (2018).

[54] A. Prakash, M. Fava, and S. A. Parameswaran, Multiversality and unnecessary criticality in one dimension (2022).

[55] H. Yao and S. A. Kivelson, Fragile mott insulators, Phys. Rev. Lett. **105**, 166402 (2010).

[56] I. P. McCulloch, Infinite size density matrix renormalization group, revisited (2008).

[57] H. N. Phien, G. Vidal, and I. P. McCulloch, Infinite boundary conditions for matrix product state calculations, Phys. Rev. B **86**, 245107 (2012).

[58] J. Haegeman, C. Lubich, I. Oseledets, B. Vandereycken, and F. Verstraete, Unifying time evolution and optimization with matrix product states, Phys. Rev. B **94**, 165116 (2016).

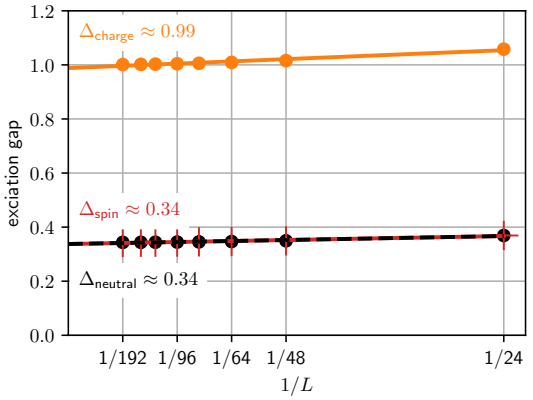

FIG. S1. Gap extrapolation for $U = V_\perp = 4, V_\parallel = 0$ for systems of length L (with $L/2$ rungs). Energies are obtained using DMRG for finite ladders with a trivial cut (unlike Fig. 5).

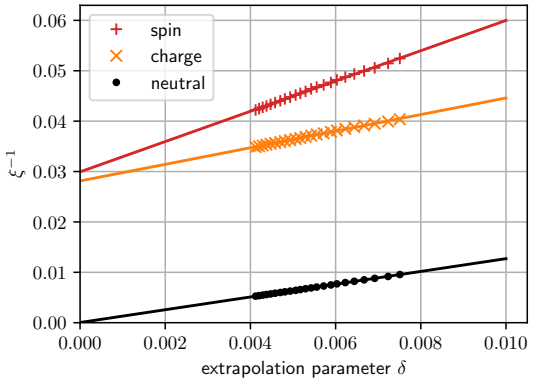

FIG. S2. Extrapolation of the inverse correlation length ξ^{-1} (measured in sites and using the trivial cut) for $U = V_\perp = 2, V_\parallel = 0$, resolved by the quantum number. The results were obtained using VUMPS for the infinite system. The extrapolation parameter δ is defined as in Ref. 50.

SUPPLEMENTAL MATERIAL

Extrapolating correlation lengths and gaps

To find the phase transition line where an excitation gap closes, we can compute the gap directly on finite systems of length L and extrapolate to the infinite limit in L^{-1}. This can be resolved by quantum number: $\Delta_{\text{spin}} = E_0\,(S = 1, N = L) - E_0\,(S = 0, N = L)$ defines the spin gap, $\Delta_{\text{charge}} = E_0\,(S = 1/2, N = L + 1) - E_0\,(S = 0, N = L)$ defines the charge gap, while $\Delta_{\text{neutral}} = E_1\,(S = 0, N = L) - E_0\,(S = 0, N = L)$ defines the neutral gap, whereby we label E_0 (E_1) the lowest (second lowest) eigenenergy in a given sector.

The result of this process is shown in Fig. S2 above the termination point, clearly showing that all gaps remain finite.

Another possibility is to compute the inverse correlation length ξ^{-1} for the infinite system, which also goes to zero at the gap closure. The correlation length is in this case obtained from the dominant eigenvalue of the transfer matrix at a fixed bond dimension χ [39, 50, 56] and can also be resolved by the same quantum numbers as above. (Note that the main text shows the neutral correlation length measured in sites rather than unit cells). One can use different extrapolation parameters δ that measure the closeness to the exact ground state (e.g. the inverse bond dimension χ^{-1}). Here, we follow Ref. 50, where a parameter was found with which $\xi^{-1}\,(\delta)$ generally becomes linear.

Figure S2 shows this procedure below the termination point. We find that the neutral correlation length vanishes, while charge and spin gaps remain open.

Microscopic analysis for the role of the operator O_j

In this section, we derive an understanding of the singlet density operator O_j in terms of the subband picture of the ladder.

We repeat the Hamiltonian in the subband basis introduced in the main text:

$$H = -t_\parallel \sum_{j,k_y,\sigma} (c^\dagger_{j,k_y,\sigma} c_{j+1,k_y,\sigma} + h.c.) - t_\perp \sum_j [n_{j,\pi} - n_{j,0}] + U/2 \sum_j [\Delta n_{j,\pi} + \Delta n_{j,0}]^2 - (U - V_\perp) H_{\text{res}}. \quad \text{(S1)}$$

Rewriting O_j in the same basis, we obtain:

$$O_j = -c^\dagger_{j,0,\uparrow} c^\dagger_{j,0,\downarrow} c_{j,\pi,\uparrow} c_{j,\pi,\downarrow} + h.c. \quad \text{(S2)}$$

We see that O_j describes the hopping of fermion pairs between the two subbands and can be used to characterize the strength of virtual scattering that violates the subband U(1) symmetry. Since the particle numbers in the subbands are conserved for $U = V_\perp$, the hopping between them must also vanish along this line: $\langle O_j \rangle = 0$.

To understand that $\langle O_j \rangle$ and $U - V_\perp$ have the same sign, we note that the residual term is given by $H_{\text{res}} = \sum_j O_j/2 + ...$, where the subband U(1) preserving terms have been neglected. Therefore, $-(U - V_\perp)\langle O_j \rangle < 0$ is expected to minimize the energy.

Similar to the above energy minimization argument for $\langle O_j \rangle$, we can argue that if there are subband U(1) violating terms breaking time-reversal symmetry (TRS) $\propto \sum_j e^{i\alpha} c^\dagger_{j,0,\uparrow} c^\dagger_{j,0,\downarrow} c_{j,\pi,\uparrow} c_{j,\pi,\downarrow} + h.c.$, the subband U(1) point can be avoided along a path connecting D-Mott to S-Mott by tuning α from 0 to π. This indicates that TRS plays an important role for the existence of a transition. This analysis is closely related to the bosonization analysis of discreetness of locking values in the main text.

As shown in the main text, the ground state $\langle n_{j,\pi}\rangle = 0$ and $\langle n_{j,0}\rangle = 1$ for $U = V_\perp \gtrsim 3.4$ ($V_{parallel} = 0$) can be written as rung bisinglet $\prod_j 1/\sqrt{2}(\Delta^\dagger_{\mathrm{S}j} + \Delta^\dagger_{\mathrm{D}j})|\Omega\rangle$. Recall from the main text that, the model wave function of D- and S-Mott ($|\mathrm{D}\rangle = \prod_j \Delta^\dagger_{\mathrm{D}j}|\Omega\rangle$ and $|\mathrm{S}\rangle = \prod_j \Delta^\dagger_{\mathrm{S}j}|\Omega\rangle$) consists rungs of two eigenstates of O operators. Consider O as an Ising field, the tendency to from rung bisinglet can be induced by transverse field, which is the counter part of the temperature in the quantum-classical analogy. This is one way to draw analogy to the magnet picture of terminable transition. However, with accidental symmetry or weak interaction, the analogy of magnetic ordering term can not emerge effectively (see the scaling dimension analysis in the main text) such that the transition is not first order as the magnetic picture.

Effective band structure

In this section, we offer a perspective on the termination of the phase transition from the perspective of an effective band structure.

The criticality at $U = V_\perp$ and its termination is related to the subband occupation ratio $\langle n_{j,\pi}\rangle / \langle n_{j,0}\rangle$ (which is not dependent on j in the homogeneous case). When this filling ratio is fractional, according to Lieb-Schultz-Mattis theorem [52, 53], the system must be gapless, unless there is a spontaneous breaking of translational symmetry resulting in a degenerate ground state.

Introducing the single-particle retarded Green's function

$$G^{ll'}\left(t, |j-j'|\right) = -i\theta(t)\Big[\sum_\sigma \langle 0|e^{iHt}c^\dagger_{jl\sigma}e^{-iHt}c_{j'l'\sigma}|0\rangle + \sum_\sigma \langle 0|e^{-iHt}c_{jl\sigma}e^{iHt}c^\dagger_{j'l'\sigma}|0\rangle\Big] \tag{S3}$$

and its Fourier transform

$$G^{ll'}(\omega, k) = \sum_d e^{ikd}\int_{-\infty}^{\infty} dt\; e^{i\omega t}G^{ll'}(t,d), \tag{S4}$$

we can define the equivalent of the bandstructure in presence of interactions by the spectral function

$$S(\omega,k) = -\frac{1}{\pi}\sum_{l=\mathrm{A,B}} \mathrm{Im}\; G^{ll}(\omega,k). \tag{S5}$$

This spectral function is displayed in Fig. S3. It reveals the two-subband structure of the ladder, whereby the lower subband has $k_y = 0$ and the upper subband has $k_y = \pi$. The parts of the subbands that lie below the Fermi edge $\omega = 0$ reflect $\langle n_{j,\pi}\rangle$ and $\langle n_{j,0}\rangle$ when integrated. In the noninteracting limit we have $\langle n_{j,\pi}\rangle / \langle n_{j,0}\rangle = 1/2$. Our calculations show that $\langle n_{j,\pi}\rangle / \langle n_{j,0}\rangle$ can change continuously along the line

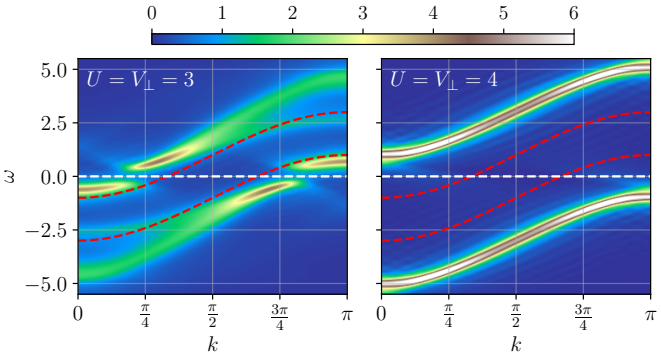

FIG. S3. The spectral function Eq. (S5). Red dashed line: band structure of the noninteracting model; white dashed line: reference for $\omega = 0$. The results are obtained by a real-time evolution of Eq. (S3) to $t_{\max} = 20$ using infinite boundary conditions [57, 58].

$U = V_\perp$. The effect of interactions is to increase the splitting of the subbands, so that for $U = V_\perp \gtrsim 3.4$, only the lower band is below the Fermi energy. This implies an integer filling $\langle n_{j,\pi}\rangle = 0$ and $\langle n_{j,0}\rangle = 1$ and the state effectively becomes a band insulator, where the two-band bosonization is no longer valid. This is why within the two-band bosonization, it is not clear that the two Mott regions can be adiabatically connected.

The bosonization of O_j

Here, we discuss the two-band bosonization of O_j. Recall that the definition is

$$O_j = -c^\dagger_{j,0,\uparrow}c^\dagger_{j,0,\downarrow}c_{j,\pi,\uparrow}c_{j,\pi,\downarrow} + h.c. \tag{S6}$$

In addition to the terms presented in the main text, we include oscillatory terms and discuss higher harmonics. Recall that the bosonization of fermion operators to the lowest harmonics is

$$c_{k_y,\sigma}(x_j) = \frac{\kappa_{k_y,\sigma}}{\sqrt{2\pi}}\sum_{\eta=-1,1} e^{i[\theta_{k_y,\sigma}+\eta(\phi_{k_y,\sigma}+k_{\mathrm{F},k_y\sigma}x_j)]}, \tag{S7}$$

We insert Eq. (S7) into Eq. (S6) to obtain the lowest harmonics of the bosonization of O_j

$$\begin{aligned} O_j \propto & \cos(2\tilde\theta_{c,-})[\cos(2\tilde\phi_{s,-}) + \cos(2\tilde\phi_{s,+}) + \\ & \cos(2\tilde\phi_{c,+} + \sum_{\sigma,k_y} k_{\mathrm{F},k_y,\sigma}x_j) + \\ & \cos(2\tilde\phi_{c,-} + \sum_\sigma (k_{\mathrm{F},\pi,\sigma} - k_{\mathrm{F},0,\sigma})x_j) + \\ & \cos(\tilde\phi_{c,+} + \tilde\phi_{c,-} + \tilde\phi_{s,+} - \tilde\phi_{s,-} + \sum_\sigma k_{\mathrm{F},0,\sigma}x_j) + \\ & \cos(\tilde\phi_{c,+} - \tilde\phi_{c,-} + \tilde\phi_{s,+} + \tilde\phi_{s,-} + \sum_\sigma k_{\mathrm{F},\pi,\sigma}x_j) + ..., \end{aligned} \tag{S8}$$

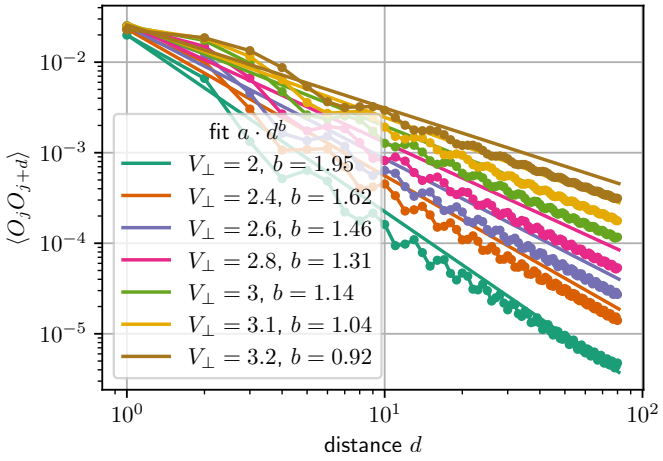

FIG. S4. Correlation function $\langle O_j O_{j+d}\rangle$ for $U = V_\perp, V_\parallel = 0$ obtained in the infinite system. The straight solid lines are references for the fitted slope of the data with the same color.

where the higher harmonics are neglected. The coefficients of each term are neglected for simplicity. At half filling, $\sum_{\sigma,k_y} k_{\mathrm{F},k_y,\sigma} = 2\pi$, which can be set to be 0, as x_j are integer. For the Mott states, as well as the D-Mott/S-Mott transition (shown to be of Gaussian type, see below), $\tilde{\phi}_{c,+}$, $\tilde{\phi}_{s,-}$,$\tilde{\phi}_{s,+}$ are kept locked and can be set to be zero for discussing expectation values or correlation function. So in this special case, we have

$$O_j \propto \cos(2\tilde{\theta}_{c,-}) + \cos(2\tilde{\theta}_{c,-})[\cos(2\tilde{\phi}_{c,-} + 2\Delta k_{\mathrm{F}} x_j) + \cos(\tilde{\phi}_{c,-} + 2k_{\mathrm{F},0,\sigma} x_j) + \cos(\tilde{\phi}_{c,-} + 2k_{\mathrm{F},\pi,\sigma} x_j)], \tag{S9}$$

where $\Delta k_{\mathrm{F}} = k_{\mathrm{F},0,\sigma} - k_{\mathrm{F},\pi,\sigma}$; for our model, $k_{\mathrm{F},k_y,\uparrow} = k_{\mathrm{F},k_y,\downarrow}$. The coefficients of each term are neglected for simplicity. These are the only two values $\tilde{\theta}_{c,-}$ can be locked at if there is no explicit or spontaneous TRS breaking; this can be seen by evaluating TRS odd term $i(c^\dagger_{j,0,\uparrow} c^\dagger_{j,0,\downarrow} c_{j,\pi,\uparrow} c_{j,\pi,\downarrow} - h.c) \propto \sin(2\tilde{\theta}_{c,-})$. In fact, $\tilde{\theta}_{c,-} \to -\tilde{\theta}_{c,-}$ for time-reversal symmetry, thus $\cos(2\tilde{\theta}_{c,-} + \alpha)$ with generic α is forbidden to appear in a time-reversal symmetric Hamiltonian. Thus, with TRS, the expected continuous transition within the 2-band effective theory is that $\tilde{\theta}_{c,-}$ becomes unlocked, indicating a Gaussian criticality. This is consistent with the microscopic argument of the TRS's role for the existence of the transition.

Correlations $\langle O_j O_{j+d}\rangle$ and Gaussian criticality

For $U = V_\perp, V_\parallel = 0$, as pointed out in the main text, the field $\tilde{\theta}_{c,-}$. and its dual field $\tilde{\phi}_{c,-}$ is gapless and characterized by a Luttinger parameter K (Eq. (5)). Here we compute $\langle O_j O_{j+d}\rangle$ using Eq. (S9) of which each term gives an algebraic decay component.

$$\langle O_j O_{j+d}\rangle = \frac{1}{|d|^{2/K}} + \frac{\cos(2k_{\mathrm{F},0,\sigma} d)}{|d|^{2/K+K/2}} + \frac{\cos(2k_{\mathrm{F},\pi,\sigma} d)}{|d|^{2/K+K/2}} + \frac{\cos(2\Delta k_{\mathrm{F}} d)}{|d|^{2/K+2K}} \tag{S10}$$

The coefficient of each term is neglected for simplicity. We see that the leading term is non-oscillatory while subleading terms can be oscillatory.

The data of $\langle O_j O_{j+d}\rangle$ for various $U = V_\perp$ are plotted in Fig. S4. We fit the exponent $2/K$ of the leading term using the log-log scale data. The fitted result for $2/K$ decreases from ~ 0.96 to ~ 0.46 as $U = V_\perp$ is increased from 2 to 3.2. From Fig. S4, we also observe subleading oscillations. In our predictions Eq. (S4), these subleading exponents are at least larger than the leading exponent by addition of $K/2$. Using the fitting result of $2/K$, this indicates that the exponent difference $K/2$ ranges from ~ 1.04 to ~ 2.17. Observing nonuniversal exponents numerically, we conclude that the transition line is of Gaussian type.

Corrected bosonization of Δ_{D} and Δ_{S}

The two-band bosonization previously reported in the literature has missed the possibility of a terminated transition. In this section, we present a corrected way of doing two-band bosonization of Δ_{D} and Δ_{S}. Recall from Eq. (2),

$$\Delta_{\mathrm{D}j} = (c_{j,\mathrm{A},\uparrow} c_{j,\mathrm{B},\downarrow} + c_{j,\mathrm{B},\uparrow} c_{j,\mathrm{A},\downarrow})/\sqrt{2},$$
$$\Delta_{\mathrm{S}j} = (c_{j,\mathrm{A},\uparrow} c_{j,\mathrm{A},\downarrow} + c_{j,\mathrm{B},\uparrow} c_{j,\mathrm{B},\downarrow})/\sqrt{2}. \tag{S11}$$

We note that Δ_{D} and Δ_{S} do not transform with different parity under any symmetry of the Hamiltonian. We aim to reconcile this fact with the fact that using bosonization, these two order parameters appear to give separate quasi-long-range orders in d- and s- paired liquids respectively. (The d-wave and s-wave states are the doped D-Mott and S-Mott respectively.) With the correction, bosonization also concludes that their existence is not mutually exclusive. We will discuss the microscopic definition of s- and d- paired liquids.

We introduce the symbols

$$\psi_{k_y,\eta,\sigma} = \frac{\kappa_{k_y,\sigma}}{\sqrt{2\pi}} e^{i(\theta_{k_y,\sigma} + \eta\phi_{k_y,\sigma})} \tag{S12}$$

for convenience. Then we can write Eq. (S7) as

$$c_{k_y,\sigma}(x_j) = \sum_{\eta=-1,1} e^{ik_{\mathrm{F},k_y\sigma} x_j} \psi_{k_y,\eta,\sigma} + ..., \tag{S13}$$

where ... represents neglected higher harmonics.

$$\Delta_{\rm S} = \sum_{\eta,\eta'=\pm1} [\psi_{0,\eta,\uparrow}\psi_{0,\eta',\downarrow} + \psi_{\pi,\eta,\uparrow}\psi_{\pi,\eta',\downarrow}] + ...,$$
$$\Delta_{\rm D} = \sum_{\eta,\eta'=\pm1} [\psi_{0,\eta,\uparrow}\psi_{0,\eta',\downarrow} - \psi_{\pi,\eta,\uparrow}\psi_{\pi,\eta',\downarrow}] + ..., \quad \text{(S14)}$$

where higher harmonic terms have been neglected. Using Eq. (S12), we obtain

$$\begin{aligned}
&\sum_{\eta,\eta'=\pm1} \psi_{0,\eta,\uparrow}\psi_{0,\eta',\downarrow} \\
&= C_0 e^{i\sum_\sigma \theta_{0,\sigma}} \cos(\phi_{0,\uparrow} - \phi_{0,\downarrow}) + ... \\
&= C_0 e^{i\sum_\sigma \theta_{0,\sigma}} [\cos(\tilde{\phi}_{+,s})\cos(\tilde{\phi}_{-,s}) - \sin(\tilde{\phi}_{+,s})\sin(\tilde{\phi}_{-,s})] + ... \\
&\sum_{\eta,\eta'=\pm1} \psi_{\pi,\eta,\uparrow}\psi_{\pi,\eta',\downarrow} \\
&= C_\pi e^{i\sum_\sigma \theta_{\pi,\sigma}} \cos(\phi_{\pi,\uparrow} - \phi_{\pi,\downarrow}) + ... \\
&= C_\pi e^{i\sum_\sigma \theta_{\pi,\sigma}} [\cos(\tilde{\phi}_{+,s})\cos(\tilde{\phi}_{-,s}) + \sin(\tilde{\phi}_{+,s})\sin(\tilde{\phi}_{-,s})] + ...
\end{aligned} \quad \text{(S15)}$$

where oscillatory terms and higher harmonics have been neglected; we explicitly write out the coefficients C_0 and C_π, which depend on parameters of Hamiltonian. The subtle issue is that with interaction, one cannot correctly obtain the values of C_0 and C_π by a naive multiplication of vertex operators' coefficients. Unlike the noninteracting limit where $C_0 = C_\pi$ because there is no exchange symmetry of π and 0 bands, we expect $C_0 \neq C_\pi$ for general interacting cases. Using the convention that $\tilde{\phi}_{-,s}$ and $\tilde{\phi}_{-,s}$ are locked at 0 for d- and s- wave paring and for the purpose of evaluating their quasi-long-range orders, Eq. (S11) can be written as

$$\Delta_{\rm S} \propto e^{i\tilde{\theta}_{+,c}}[C_0\cos(\tilde{\theta}_{-,c}) + (C_\pi - C_0)e^{i\tilde{\theta}_{-,c}}] + ...$$
$$\Delta_{\rm D} \propto e^{i\tilde{\theta}_{+,c}}[C_0\sin(\tilde{\theta}_{-,c}) - (C_\pi - C_0)e^{i\tilde{\theta}_{-,c}}] + ..., \quad \text{(S16)}$$

In the convention, $\tilde{\theta}_{-,c}$ is locked at 0 and $\pi/2$ for s- and d-pairing states respectively. Thus if $C_0 = C_\pi$, only quasi-long-range order of $\Delta_{\rm S}$ exists for s-wave states; the same applies to d-wave. Given that $C_0 \neq C_\pi$ in general, we have both quasi-long-range orders in either s- and d-wave states; in other words, $\langle \Delta_{{\rm S}j}\Delta^\dagger_{{\rm S},j+d}\rangle$ and $\langle \Delta_{{\rm D}j}\Delta^\dagger_{{\rm D},j+d}\rangle$ decay algebraically in $|d|$ with the same exponent. However, we can still have a microscopic definition of s-wave and d-wave states. If the leading algebraic decay prefactor of $\langle \Delta_{{\rm S}j}\Delta^\dagger_{{\rm S},j+d}\rangle$ is larger, we call the state s-wave, otherwise d-wave. This is equivalent to the definition from the relative sign of the coefficient of the leading algebraic decay components of $\langle \Delta_{0,{\rm j}}\Delta^\dagger_{0,{\rm j+d}}\rangle$ and $\langle \Delta_{\pi,{\rm j}}\Delta^\dagger_{\pi,{\rm j+d}}\rangle$, where $\Delta_{{\rm k_y,j}} = c_{j,k_y,\uparrow}c_{j,k_y,\downarrow}$ A positive relative sign is defined as s-wave states and a negative relative sign is defined as d-wave states. Such a definition no longer necessitates a transition between s- and d-states. A definition via the sign is closely related to our definition of S- and D-Mott using the sign of $\langle O_j\rangle$.

Analytical solution for a single rung

In this section, we discuss the analytical solution of a single rung at half filling (which amounts to analyzing a 4×4 matrix) and discuss what one can learn from it for the full model.

The Hamiltonian on a single rung can be written as:

$$\begin{aligned}
H_{\rm rung} = &-t_\perp \sum_\sigma \left(c^\dagger_{{\rm A}\sigma}c_{{\rm B}\sigma} + h.c.\right) \\
&+ U\left(n_{{\rm A}\uparrow}n_{{\rm A}\downarrow} + n_{{\rm B}\uparrow}n_{{\rm B}\downarrow}\right) \\
&+ V_\perp \sum_{\sigma\sigma'} n_{{\rm A}\sigma}n_{{\rm B}\sigma'} + V_\perp - V_\perp \sum_\sigma \left(n_{{\rm A}\sigma} + n_{{\rm B}\sigma}\right).
\end{aligned} \quad \text{(S17)}$$

At half filling we can replace $\sum_\sigma (n_{{\rm A}\sigma} + n_{{\rm B}\sigma}) = 2$ and use the basis states $c^\dagger_{{\rm A}\uparrow}c^\dagger_{{\rm B}\downarrow}|\Omega\rangle = |\uparrow,\downarrow\rangle$, $c^\dagger_{{\rm A}\downarrow}c^\dagger_{{\rm B}\uparrow}|\Omega\rangle = |\downarrow,\uparrow\rangle$, $c^\dagger_{{\rm A}\uparrow}c^\dagger_{{\rm A}\downarrow}|\Omega\rangle = |\uparrow\downarrow,0\rangle$, $c^\dagger_{{\rm B}\downarrow}c^\dagger_{{\rm B}\uparrow}|\Omega\rangle = |0,\uparrow\downarrow\rangle$, whereby $|\Omega\rangle$ is the vacuum. In this basis, the Hamiltonian matrix reads:

$$H = \begin{pmatrix} 0 & 0 & -t_\perp & -t_\perp \\ 0 & 0 & +t_\perp & +t_\perp \\ -t_\perp & +t_\perp & U - V_\perp & 0 \\ -t_\perp & +t_\perp & 0 & U - V_\perp \end{pmatrix}. \quad \text{(S18)}$$

This is a two-site Hubbard problem, extended by $V_\perp$. We see that for a single rung, its effect is to simply shift $U \to U - V_\perp$ (which is not generally true for the full ladder). The eigenstates can be characterized by the spin and pseudospin quantum numbers (which we call "S" and "T", respectively), whereby the pseudospin operators for a bipartite lattice are in general defined as:

$$\begin{aligned}
T^+_i &= (-1)^i c_{i\downarrow}c_{i\uparrow}, \\
T^+_i &= (-1)^i c^\dagger_{i\uparrow}c^\dagger_{i\downarrow}, \\
T^z_i &= \frac{1}{2}(n_i - 1),
\end{aligned} \quad \text{(S19)}$$

and fulfill SU(2) algebra relations $\left[T^z_i, T^\pm_j\right] = \pm\delta_{ij}T^\pm_i$, $\left[T^+_i, T^-_j\right] = 2\delta_{ij}T^z_i$. For a single rung the indices are $i, j = {\rm A}, {\rm B}$.

Two of the four eigenstates are the spin-triplet and the pseudospin-triplet:

- spin-triplet:
  $|S = 1, M_S = 0\rangle = \frac{1}{\sqrt{2}}\left(|\uparrow,\downarrow\rangle + |\downarrow,\uparrow\rangle\right)$
  $E = 0$
- pseudospin-triplet:
  $|T = 1, M_T = 0\rangle = \frac{1}{\sqrt{2}}\left(|0,\uparrow\downarrow\rangle - |\uparrow\downarrow,0\rangle\right)$
  $E = U - V_\perp$

The corresponding singlets are:

- spin-singlet:
  $|S = 0\rangle = \frac{1}{\sqrt{2}}\left(|\uparrow,\downarrow\rangle - |\downarrow,\uparrow\rangle\right)$

- pseudospin-singlet:
  $\big|T=0\big\rangle = \frac{1}{\sqrt{2}}\left(\big|0,\uparrow\downarrow\big\rangle + \big|\uparrow\downarrow,0\big\rangle\right)$

However, they are not by themselves eigenstates. Instead, one needs to form a "bonding" and and an "antibonding" superposition:

- bonding singlet superposition:
  $\big|S=T=0,-\big\rangle = \alpha_-\big|S=0\big\rangle + \beta_-\big|T=0\big\rangle$
  $E_- = \frac{U-V_\perp}{2} - \sqrt{\left(\frac{U-V_\perp}{2}\right)^2 + 4t_\perp^2}$
- antibonding singlet superposition:
  $\big|S=T=0,+\big\rangle = \alpha_+\big|S=0\big\rangle + \beta_+\big|T=0\big\rangle$
  $E_+ = \frac{U-V_\perp}{2} + \sqrt{\left(\frac{U-V_\perp}{2}\right)^2 + 4t_\perp^2}$

The mixing coefficients are given by:

$$\begin{aligned}\alpha_\pm &= \frac{1}{\sqrt{1+E_\pm^2/(4t_\perp^2)}},\\ \beta_\pm &= -\frac{E_\pm}{2t_\perp}\frac{1}{\sqrt{1+E_\pm^2/(4t_\perp^2)}}.\end{aligned} \tag{S20}$$

The bonding singlet superposition is always the ground state. It contains more spin-singlets in the admixture for $U > V_\perp$ (which becomes the D-Mott phase on the ladder), more "pseudo-singlets" (on-site singlets) for $U < V_\perp$ (which becomes the S-Mott phase); and an equal superposition $\frac{1}{\sqrt{2}}\left(\big|S=0\big\rangle + \big|T=0\big\rangle\right)$ for $U = V_\perp$, which we call a "rung bisinglet" in the main text.

In the strong-coupling limit $\big|U - V_\perp\big| \gg t_\perp$ and for $U > V_\perp$, we have $E_- \approx -4\frac{t_\perp^2}{U-V_\perp} = J$, and the two low-lying states become the spin-singlet and spin-triplet, split in energy by J, indicating an effective Heisenberg model.

On the other hand, if $V_\perp < U$, we obtain $E_- \approx U - V_\perp + J$ and the two low-lying states become the pseudospin singlet and pseudospin triplet, again split in energy by J. We see that even though the density-density interaction of the original model is of Ising type and only couples the z-components of the pseudospin, the strong-coupling limit favors entangled singlet states. This is because we have restricted ourselves to half filling for the rung, where $V_\perp$ acts exactly as an attractive $U < 0$.

For the full ladder, both $V_\perp > 0$ and $U < 0$ favor an S-Mott phase, but the effect of $V_\perp$ cannot be simply captured by substituting $U \to U - V_\perp$. Doing so neglects charge fluctuations on the rungs and will not reveal the terminated transition.